Catalysis Science & Technology

Accepted Manuscript

ROYAL SOCIETY OF CHEMISTRY

www.rsc.org/catalysis

Enhanced photocatalytic activity of Pt/WO_3 photocatalyst combined with TiO_2 nanoparticles by polyelectrolyte-mediated electrostatic adsorption

Tomomi Ohashi, Takashi Sugimoto, Kaori Sako, Shinjiro Hayakawa, Kiyofumi Katagiri,* and Kei Inumaru*

Department of Applied Chemistry, Graduate School of Engineering, Hiroshima University, 1-4-1 Kagamiyama, Higashi-Hiroshima, Hiroshima 739-8527, Japan

Abstract

An electrostatic adsorption approach was used to realize a composite structure in which larger metal oxide crystalline particles were surrounded by metal oxide nanoparticles. Poly(diallyldimethylammonium chloride) (PDDA) and poly(sodium 4-styrenesulfonate) were alternatingly adsorbed on to crystalline tungsten trioxide (WO_3) particles (ca. 200 nm) *via* layer-by-layer assembly, followed by adsorption of TiO_2 particles (ca. 6 nm) on the surfaces covered by PDDA. After calcination to remove the adsorbed polymer layers, Pt particles were dispersed on the composite structure by photodeposition. The resulting Pt/WO_3-TiO_2 composite photocatalyst showed a higher rate of activity towards the photocatalytic decomposition of gaseous acetone under visible light irradiation ($\lambda > 420$ nm) compared with that of Pt/WO_3. Pt/WO_3-TiO_2 also converted acetone to CO_2 almost completely, whereas the amount of CO_2 produced over Pt/WO_3 was much smaller than that expected for the complete oxidation of acetone. The enhanced activity of Pt/WO_3-TiO_2 was ascribed to hole transfer from the valence band of WO_3 to that of TiO_2, which likely suppressed electron-hole recombination and enabled the oxidation reaction to take place on the surface of the TiO_2 particles.

Keywords: WO_3, TiO_2, nanocomposite, visible light, air, purification

* Corresponding authors

K. Katagiri, kktgr@hiroshima-u.ac.jp

K. Inumaru, inumaru@hirohsima-u.ac.jp

TOC Entry:

An electrostatic adsorption approach was used to realize a composite structure in which larger WO_3 crystalline particles were surrounded by TiO_2 nanoparticles. The Pt/WO_3-TiO_2 composite photocatalyst showed a high activity under visible light irradiation ($\lambda > 420$ nm).

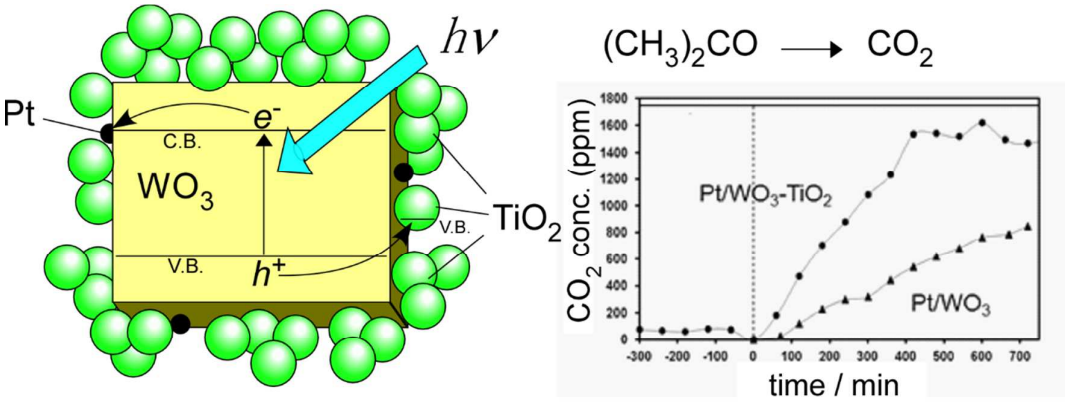

Introduction

Nanostructural control of composite materials to achieve enhanced functions has been of great interest in the fields of catalyst and photocatalyst design.[1,2] Various nanomaterials have been investigated such as nanoparticles,[3-5] nanofibers,[6,7] and nanoporous materials.[8-12] The design of composite materials is also a promising strategy to achieve novel functions in this area, and nanocomposite structures are important subjects of recent studies on photocatalysts.[9-12] For example, composite photocatalysts of TiO_2 combined with mesoporous silica showed molecule selective photocatalytic activity toward the decomposition of organic molecules in water.[11,12] Furthermore, Z-scheme photocatalysis has been achieved by combining different metal oxides to create systems in which one metal oxide passes electrons to the other.[13,14]

WO_3 has recently attracted much attention as a visible light sensitive photocatalyst. Abe et al. found that platinum-loaded WO_3 (Pt/WO_3) showed high photocatalytic activity for the oxidation of organic molecules under visible light irradiation.[15] In this system, electrons excited to the conduction band (CB) of WO_3 move to Pt particles and multi-electron reduction reactions proceed on the Pt, achieving visible light sensitivity and high photocatalytic activity. Composite materials containing WO_3 and TiO_2 have recently been investigated extensively.[16-22] In the early stages of such research, Miyauchi and Hashimoto et al. reported a WO_3–TiO_2 bilayer structure showing high photoinduced hydrophilic properties.[21] In this system, holes generated in the valence band (VB) of WO_3 transfer to the VB of TiO_2 and electrons excited to the CB of TiO_2 transfer to the CB of WO_3, enhancing the efficiency of charge separation and the hydrophilic properties of the surface. A $Pt/WO_3/TiO_2$ tri-layer structure prepared by sputtering has been applied to the photocatalytic decomposition of organic molecules in air.[22] The thin film photocatalyst showed high activity because of enhanced charge separation efficiency. An important process in these systems is the transfer of electrons and holes through the interfaces between WO_3 and TiO_2. Thus, the design of such interfaces is a fundamental and interesting aspect of achieving enhanced photocatalytic performance.

In this study, we constructed a nanostructure in which well-crystallized TiO_2 nanoparticles (ca. 6 nm) were adsorbed onto the surface of larger WO_3 crystals (ca. 200 nm). The WO_3-TiO_2 interfaces were formed by an electrostatic adsorption technique. Pt was deposited on the composite to form a Pt nanoparticles / WO_3 crystals / TiO_2 crystalline particles structure. The photocatalytic performance of the composite material was investigated and is discussed in terms of the nanostructure of and interfaces between the two different metal oxides.

Experimental

Materials

$Na_2WO_4 \cdot 2H_2O$, 20 wt% poly(diallyldimethylammonium chloride) (PDDA) and poly(sodium 4-styrene sulfonate) (PSS) were purchased from Sigma Aldrich. Hydrochloric acid (35 wt%), methanol and acetone were purchased from Nacalai Tesque (Tokyo, Japan). Tartaric acid was obtained from Kishida Chemical Co., Ltd. (Tokyo, Japan). TiO_2 sol (TKS-203, anatase form, 20.1 wt%) was kindly supplied by Tayca Co., Ltd. (Osaka, Japan). All of the reagents were used without further purification.

Preparation of photocatalysts

Plate-like WO_3 crystals were prepared according to the literature.[23] 0.99 g of $Na_2WO_4 \cdot 2H_2O$ and 2.09 g of tartaric acid were added to 15 cm^3 of 35 wt% HCl mixed with 30 cm^3 of pure water. The resulting solution was ultrasonically treated for 1 h, charged into an autoclave, and then heated at 433 K for 24 h. The obtained precipitate was separated by centrifugation and alternatingly washed with water and ethanol three times. The resulting solid was then calcined in air at 623 K (heating rate 5 K min^{-1}) for 4 h. WO_3 particles with irregular morphology were also prepared by another method. A solution of 1 M $Na_2WO_4 \cdot 2H_2O$ (25 cm^3) and a solution of 3 M HCl (225 cm^3) were combined at 373 K and was stirred for 30 min. The precipitation was filtered, dried and calcined at 773 K for 2h. This sample was designated as WO_3-ir.

The obtained WO_3 crystals were dispersed in water (20 g dm^{-3}). Solutions of each of poly(diallyldimethylammonium chloride) (PDDA) and poly(sodium 4-styrene sulfonate) (PSS) were prepared using an aqueous 0.5 mol dm^{-3} NaCl solution. The concentrations of the polymers were adjusted to 1 mg cm^{-3}. 5 cm^3 of the WO_3 dispersion was separated by centrifugation, and 5 cm^3 of the PDDA solution was added to the centrifuge vessel, followed by vigorous mixing using a vortex mixer. After standing for 15 min, the solid was separated by centrifugation and washed with water three times. Next, 5 cm^3 of the PSS solution was added to the solid. The two procedures were repeated several times for the layer-by-layer deposition of the polymers. Finally, 5 cm^3 of dilute TiO_2 sol (1 wt%) was added to the solid covered by PDDA for electrostatic adsorption of TiO_2. The solid was then washed with water three times, dried and calcined at 773 K for 2 h (heating rate 1 K min^{-1}). Pt was loaded on the resulting samples by photodeposition. 0.1 g of sample was dispersed in 10 cm^3 of pure water and outgassed using bubbling N_2 gas for 2 h. 13.3×10^{-3} cm^{-3} of a 0.193 M aqueous solution of H_2PtCl_4 and 1.1 cm^{-3} of CH_3OH were then added to the suspension. The mixture was photoirradiated with a 500 W Xe lamp. For comparison, the Pt photodeposition was carried out on an additional sample using an L420 cut filter.

Characterization

X-ray powder diffraction patterns were measured with a D8 Advance diffractometer (Bruker AXS) using Cu Kα radiation (Ni filtered). An in-house made X-ray fluorescence spectrometer was used to

determine the TiO_2 content of the sample. SEM and TEM images were taken with an S-4800 microscope (Hitachi) and a JEM-2010 microscope (JEOL), respectively. ζ-Potentials were measured with a ELSZ-2 (Otsuka Electric Co.).

Photocatalytic test

The procedure used to measure the photocatalytic decomposition of gaseous acetone has been described in detail elsewhere.[24,25] A glass vessel (Nichiden-Rika Glass Co., Ltd. SV-100, 113.8 cm^3) was used as the reactor. The photocatalyst sample (30 mg) was placed on an area of 1.5 cm × 2.0 cm of a glass plate, and plate was placed in the reactor. The reactor was then irradiated with a 500 W Xe lamp (JASCO Co.) overnight to completely convert organic species in the reactor to CO_2. The lamp was turned off and 2.71×10^{-6} mol of acetone, equivalent to 583 ppm, was injected into the reactor. The gas phase in the reactor was sampled with a syringe and analyzed using a GC equipped with an FID detector (Shimadzu GC-2014). After the adsorption had reached equilibrium, the reactor was irradiated again with the Xe lamp. An L420 filter was used to cut out light with wavelength shorter than 420 nm. The time courses of the concentrations of acetone and CO_2 were monitored with the GC. A methanizer (Shimadzu MTN-1) was used for analysis of CO_2. CO_2 concentration was expressed after subtraction of its concentration at time zero (*ca*. 1000 ppm).

Estimation of quantum efficiency

The light power irradiated to the photocatalyst through L42 filter was measured with a radiometer (Topcon UVR-300 with a detector UD400; sensible wavelength range 360-490 nm). The value was 2.2 mW cm^{-2}. Considering the area of photocatalyst in the reactor (3.0 cm^2) and minimum photon energy that WO_3 can absorb (2.6 eV; 477 nm), the maximum number of photons having energy larger than 2.6 eV irradiated to the photocatalyst was roughly estimated. Based on this value, the approximate apparent quantum efficiency was calculated.

Results

Fig. 1 shows the variation in the ζ-potential of the samples during the layer-by-layer adsorption process. The pristine WO_3 crystals had a negative potential of ca. −40 mV. After the first addition of PDDA, the ζ-potential became positive, indicating electrostatic adsorption of PDDA molecules on the surface of the WO_3. Then, PSS and PDDA were alternately adsorbed on the surface of the sample to form five layers of the polymers in total (3 layers of PDDA and 2 layers of PSS). During these processes, the sign of the ζ-potential alternated correspondingly. The second and the third PDDA adsorption resulted in similar positive potentials of ca. 50 mV, which seemed to reach a stable level. This suggests that the PDDA molecules fully covered the surface of the sample. It is well known that the alternating adsorption of the polymers forms a "precursor-layer", which is

important to form effective surface charge for well-reproducible electrostatic adsorption of particles.[26-28] Finally, the sample was subjected to adsorption of TiO_2 nanoparticles using the TiO_2 sol. The potential changed to a negative value of ca. −30 mV, indicating that the surface of the sample was well covered by negatively charged TiO_2 nanoparticles.

Electron microscope images of the samples are presented in Fig. 2. Fig. 2a and b show SEM and TEM images of the pristine WO_3 crystals, respectively. Thick plate-like crystals of ca. 200 nm in width were observed. Fig. 2c shows a TEM image of the sample after adsorption of TiO_2 nanoparticles (before calcination). The WO_3 crystals were clearly completely surrounded by TiO_2 nanoparticles, which appeared to form aggregates of ca. 20–50 nm in size. These aggregates were closely attached to the surfaces of the WO_3 crystals. The sample was calcined at 773 K in air to remove the polymer layers on the WO_3 surfaces. Fig. 2d presents a TEM image of the TiO_2-adsorbed sample after calcination. The higher magnification image confirmed that close contact between WO_3 and TiO_2 was maintained after the calcination.

Fig. 3 shows the X-ray diffraction (XRD) patterns of the samples prepared in this study. Fig. 3a is the diffraction pattern of the powder obtained after drying the TiO_2 sol. The clear peaks were all assignable to the anatase TiO_2 crystal structure. The peaks in the XRD pattern of the pristine WO_3 (not shown) were all ascribed to monoclinic WO_3. A weak peak of anatase TiO_2 was observed in the XRD pattern of the TiO_2-adsorbed sample in addition to the diffraction peaks of WO_3 (Fig. 3b and its inset). X-ray fluorescence analysis revealed that the sample contained a small amount of TiO_2 (6 wt%). This is the reason why only the main XRD peak of anatase was observed in the diffraction pattern of the TiO_2 adsorbed sample (Fig. 3b). According to these results, the electrostatic adsorption technique successfully realized a structure in which WO_3 crystals were completely surrounded by and in close contact with TiO_2 nanoparticles.

The photocatalytic activity of the samples was tested using the decomposition of gaseous acetone under visible light irradiation. Fig. 4 presents the results obtained for the Pt/WO_3-TiO_2 composite photocatalyst. For comparison, the results for Pt/WO_3 are also presented in the same figure. In the time course of acetone concentration (Fig. 4a), adsorption equilibrium was achieved at the initial stage before the photoirradiation was begun. The amount of acetone introduced to the reactor corresponded to 583 ppm; the differences between the equilibrium concentration and this value are attributed to adsorption of the acetone onto the surface of the photocatalyst. Pt/WO_3-TiO_2 showed a larger adsorption acetone than Pt/WO_3. This is probably because the considerable surface area of the TiO_2 nanoparticles contained in Pt/WO_3-TiO_2 meant that a larger amount of acetone was removed from the gas phase than in the case of Pt/WO_3. After the photoirradiation, Pt/WO_3-TiO_2 decomposed acetone faster than Pt/WO_3 did. The difference in the reaction rates is clearly demonstrated in the first order plots of acetone concentration (Fig. 5).

The difference between the activities of the two photocatalysts is more obvious in the time

course of CO_2 concentration (Fig. 4b). For Pt/WO_3, CO_2 generation was slow and the concentration produced was much lower than that expected for the complete oxidation of acetone (1749 ppm), even when acetone had disappeared from the gas phase (700 min after the start of photoirradiation). In contrast, Pt/WO_3-TiO_2 generated CO_2 much more quickly, and the concentration of CO_2 reached the level close to that expected for complete oxidation of acetone when acetone in the gas phase disappeared. That is, Pt/WO_3–TiO_2 with TiO_2 nanoparticles decomposed acetone completely to CO_2, and its photocatalytic activity was much higher than that of Pt/WO_3. For comparison, TiO_2 sol was dried and tested for the photocatalytic decomposition of acetone. The TiO_2 showed very low activity under the same test conditions (not shown), demonstrating that combination of Pt/WO_3 and TiO_2 is indispensable to the enhanced activity under visible light irradiation. Furthermore, an additional type of composite photocatalyst was prepared and compared, where an L420 cutoff filter was used during the photodeposition of Pt onto the composite. The photocatalyst prepared without an L420 filter must have Pt particles on both the WO_3 crystal and TiO_2 nanoparticles, whereas the photocatalyst prepared using an L420 filter, the Pt must exist only on WO_3. The photocatalytic activity of the two different composite photocatalysts were very similar (not shown) under photoirradiation through an L420 filter. This is reasonable because TiO_2 particles cannot be photoexcited under these conditions. The decomposition of acetone over the TiO_2 under the same conditions was negligibly slow. These results demonstrate that a combination of Pt/WO_3 and TiO_2 is indispensable to the enhanced activity observed in the present work. Pt/WO_3-ir – TiO_2, a composite photocatalyst prepared from WO_3 having irregular morphology (WO_3-ir) showed lower activity compared to Pt/WO_3-TiO_2 but still have higher activity than Pt/WO_3, showing wide versatility of the present method.

Discussion

Electrostatic adsorption was successfully used to prepare WO_3 crystals surrounded by TiO_2 nanoparticles, as shown in Fig. 2c. The primary particles of the TiO_2 were ca. 6 nm in size, but formed aggregates of ca. 20 nm in size (Fig. 2d). These aggregates closely contacted the surfaces of the WO_3 crystals.

The composite catalyst Pt/WO_3-TiO_2 showed enhanced photocatalytic activity for the photodecomposition of gaseous acetone compared with that of Pt/WO_3. In particular, the amount of CO_2 generated over Pt/WO_3 was much less than that over Pt/WO_3-TiO_2. In other words, Pt/WO_3-TiO_2 showed superior performance in the total oxidation of acetone, whereas Pt/WO_3 could not decompose acetone completely to CO_2. It was confirmed that TiO_2 alone could not decompose acetone under the same conditions. These results have demonstrated that the combination of Pt/WO_3 and TiO_2 is essential for enhanced photocatalytic activity in complete acetone oxidation. It has been claimed that combination of WO_3 and TiO_2 allows transfer of holes from the VB of WO_3 to that of

TiO_2.[21] In the present study, light with wavelength longer than 420 nm was used for the photocatalytic reaction. Thus, the WO_3 was able to absorb photons and generate excited electrons in its CB and holes in its VB, while the TiO_2 could not absorb the light. If the holes in the VB of WO_3 transferred to the VB of TiO_2, the recombination of electrons and holes would have been suppressed (Fig. 6) and the holes would contribute to the oxidation reaction on the surface of the TiO_2 particles.

As described in the experimental section, using the light power measured with the radiometer and minimum photon energy that WO_3 can absorb (2.6 eV), the maximum number of photon (> 2.6 eV) was estimated. The value was 1.1×10^{15} photon s^{-1}. Here we assumed that H_2O_2 and hydroxyl radicals were produced by multielectron reduction of oxygen and reaction of hydroxyl anions with positive holes, respectively. Supposing that these all contribute to the decomposition of acetone, we calculated the minimum value of the apparent quantum efficiency to be 3.8 % based on the CO_2 evolution rate shown in Fig. 4. Considering possible error of the light power measurement, we concluded that the approximate apparent quantum efficiency was several percent or above in our experiments. It was reported that Fe(III) or Cu(II)-modified TiO_2 could achieved quantum efficiency as high as 92.2 % for 2-propanol decomposition.[29] The apparent quantum efficiency of Pt/WO_3-TiO_2 was 2.5 times higher than that of Pt/WO_3, when it was estimated from the CO_2 evolution rates in Fig. 4.

Conclusions

An electrostatic adsorption approach was successfully used to construct a composite structure in which larger WO_3 crystalline particles were surrounded by TiO_2 nanoparticles. The resulting Pt/WO_3-TiO_2 composite photocatalyst showed enhanced photocatalytic activity toward the decomposition of gaseous acetone under visible light irradiation. The Pt/WO_3-TiO_2 showed enhanced activity for acetone decomposition and converted the acetone to CO_2 almost completely, in contrast to Pt/WO_3 which produced a much smaller amount of CO_2 than that expected for the complete oxidation of acetone. The enhanced activity of Pt/WO_3-TiO_2 was ascribed to the transfer of holes from the VB of WO_3 to that of TiO_2, which may have suppressed electron-hole recombination and enabled the oxidation reaction to occur on the surface of the TiO_2. This work highlights a promising strategy for constructing nano-structured composite photocatalysts by using an electrostatic adsorption approach.

Acknowledgments

This work was supported by the Advanced Catalytic Transformation Program for Carbon Utilization

(ACT–C), Japan Science and Technology Agency (JST), by Asahi-glass foundation, and by Grants-in-Aid for Scientific Research (B) from Japan Society for the Promotion of Science, and partially by a Grant-in-Aid for Scientific Research (No. 22107011) on the Innovative Areas: "Fusion Materials: Creative Development of Materials and Exploration of Their Function through Molecular Control" (Area no. 2206) from the Ministry of Education, Culture, Sports, Science and Technology (MEXT). The authors thank Dr. M. Maeda for TEM measurements.

References

1 S. L. Suib (Ed.), *New and Future Development in Catalysis, Hybrid Materials, Composite, and Organocatalysts*, Elsevier, Amsterdam, 2013.

2 A. Kubacka, M. Fernández-García, G. Colón, *Chem. Rev.* **112**, 1555-1614 (2012).

3 M. Murodoch, G. I. N. Watherhouse, M. A. Nadeem, J. B. Metson, M. A. Keane, R. F. Howe, J. Llorca, H. Idress, *Nature Chem.* **3**, 489-492 (2011).

4 K. Katagiri, Y. Miyoshi, K. Inumaru, *J. Colloid Interface Sci.*, **407**, 282-286 (2013).

5 K. Katagiri, R. Takabatake, K. Inumaru, *ACS Appl. Mater. Interfaces,* **5**, 10240-10245 (2013).

6 S.-K. Choi, S. Kim, S.-K. Lim, H. Park, *J. Phys. Chem. C,* **114**, 16475-16480 (2010).

7 Z. Y. Zhang, C. L. Shao, X. H. Li, C. H. Wang, M. Y. Zhang, Y. C. Liu, *ACS Appl. Mater. Interfaces,* **2**, 2915-2923 (2010).

8 Y. Ren, Z. Ma, P. G. Bruce, *Chem. Soc. Rev.* **41**, 4906-4927 (2012).

9 K. Inumaru, T. Ishihara, K. Kamiya, T. Okuhara, S. Yamanaka, *Angew. Chem. Int. Ed.* **46**, 7625-7628 (2007).

10 T. Kasahara, K. Inumaru, S. Yamanaka, *Micropor. Mesopor. Mater.* **76**, 123-130 (2004).

11 K. Inumaru, T. Kasahara, M. Yasui, S. Yamanaka, *Chem. Commun.*, 2131-2133 (2005).

12 K. Inumaru, M. Yasui, T. Kasahara, K. Yamaguchi, Y. Yasuda, S. Yamanaka, *J. Mater. Chem.* **21**, 12117-12125 (2011).

13 A. Kudo, *MRS Bull.* **36**, 32-38 (2011).

14 Y. Sakai, H. Nemoto, K. Saito, A. Kudo, *J. Phys. Chem. C*, **113**, 17536 (2009).

15 R. Abe, H. Takami, N. Murakami, B. Ohtani, *J. Am. Chem. Soc.,* **130**, 7780-7781 (2008).

16 Y. R. Do, W. Lee, K. Dwight, A. Wold, *J. Solid State Chem.* **108**, 198-201 (1994).

17 T. Ohno, F. Tanigawa, K. Fujihara, S. Izumi, M. Matsumura, *J. Photochem. Photobiology A-Chem.* **118**, 41-44 (1998).

18 Y.-T. Kwon, K.-Y. Song, W.-I. Lee, G.-J. Choi, Y.-R. Do, *J. Catal.*, **191**, 192-199 (2000).

19 K. K. Akurati, A. Vital, J. P. Dellemann, K. Michalow, T. Graule, D. Fetti, A. Baiker, *Appl. Catal. B* **79**, 53-62 (2008).

20 D. Tsukamoto, M. Ikeda, Y. Shiraishi, T. Hara, N. Ichikuni, S. Tanaka, T. Hirai, *Chem. Eur. J.*,

35, 9816-9824 (2011).

21 M. Miyauchi, A. Nakajima, T. Watanabe, K. Hashimoto, *Chem. Mater.*, **14**, 4714-4720 (2002).

22 A. Srinivasan, M. Miyauchi, *J. Phys. Chem. C*, **116**, 15421-15426 (2012).

23 X. G. Han, X. Han, L. Li, C. Wang, *New J. Chem.* **36**, 2205-2208 (2012).

24 B. Ohtani, *Hikarishokubai Hyojun Kenkyuho* (Standard research methods of photocatalysts), 2005, Tokyo Tosho, Tokyo, Japan (ISBN 4-489-00697-7), p112.

25 H. Sakai, Y. Kubota, K. Yamaguchi, H. Fukuoka, K. Inumaru, *J. Porous Mater*. **20**, 693-699 (2013).

26 C. Peng, Y. S. Thio, R. A. Gerhardt, *Langmuir* **28**, 84-91 (2012).

27 Y. Lvov, K. Ariga, M. Onoda, I. Ichinose, T. Kunitake, *Langmuir* **13**, 6195-6203 (1997).

28 F. Caruso, H. Möhwald, *Langmuir* **15**, 8276-8281 (1999).

29 M. Liu, M. Nishikawa, X. Qiu, D. Atarashi, E Sakai, Y. Nosaka, K. Hashimoto, M. Miyauchi, *ACS Nano*, **8**, 7229-7238 (2014).

Figure captions

Fig. 1 Variation of ζ-potential during electrostatic adsorption process.

Fig. 2 Microscope images of the samples. (a) SEM image of pristine WO_3, (b) TEM image of pristine WO_3, (c) TEM images of WO_3 after adsorption of TiO_2 nanoparticles. (d) TEM image after removal of organic polymer layers by calcination.

Fig. 3 X-ray powder diffraction pattern of (a) dried TiO_2 sol and (b) Pt/WO_3-TiO_2. Inset shows the magnified pattern and the red circle indicates the main diffraction peak of the anatase TiO_2 phase.

Fig. 4 Time courses of acetone and CO_2 concentrations during the photocatalytic reaction.

Fig. 5 First order plot of acetone concentration during the photocatalytic reaction. Solid circles; Pt/WO_3-TiO_2, solid triangles; Pt/WO_3.

Fig. 6 Schematic illustration of composite photocatalyst.

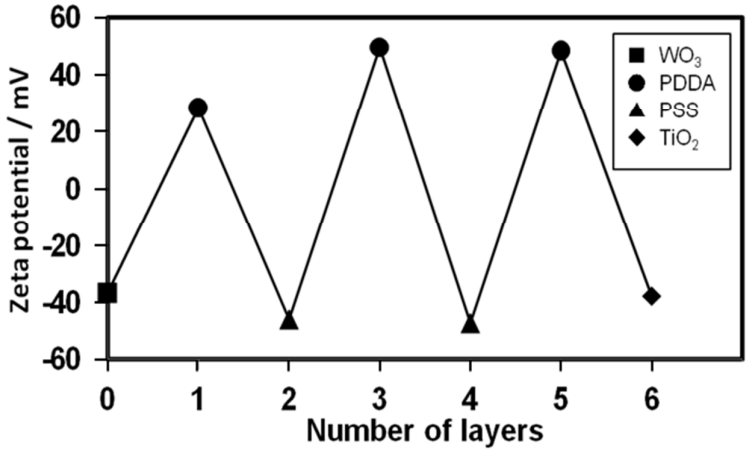

Fig. 1 Variation of ζ-potential during electrostatic adsorption process.

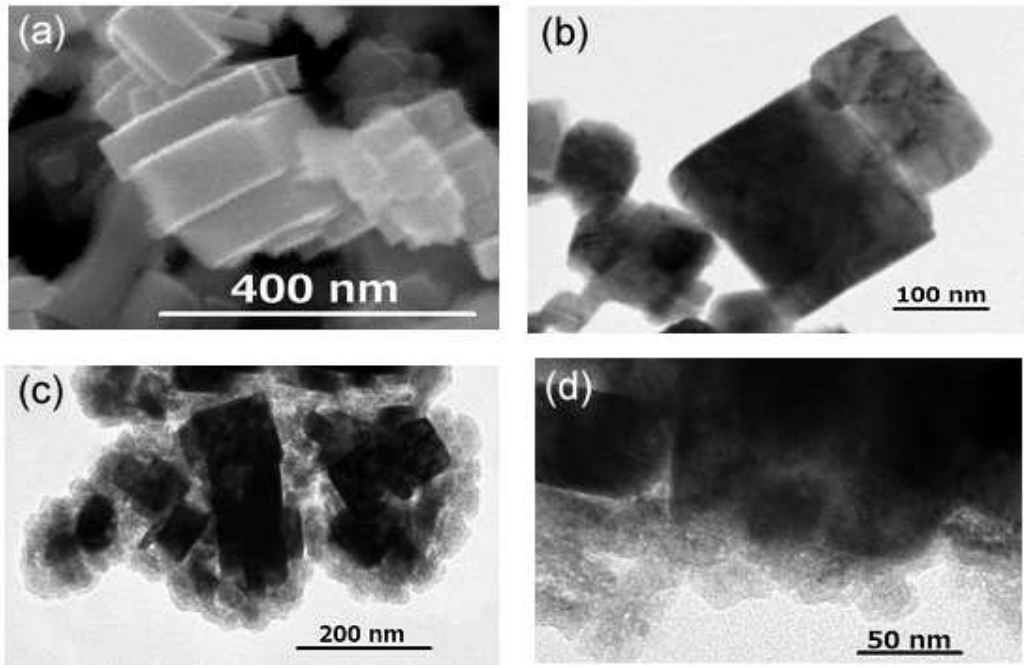

Fig. 2 Microscope images of the samples. (a) SEM image of pristine WO_3, (b) TEM image of pristine WO_3, (c) TEM images of WO_3 after adsorption of TiO_2 nanoparticles. (d) TEM image after removal of organic polymer layers by calcination.

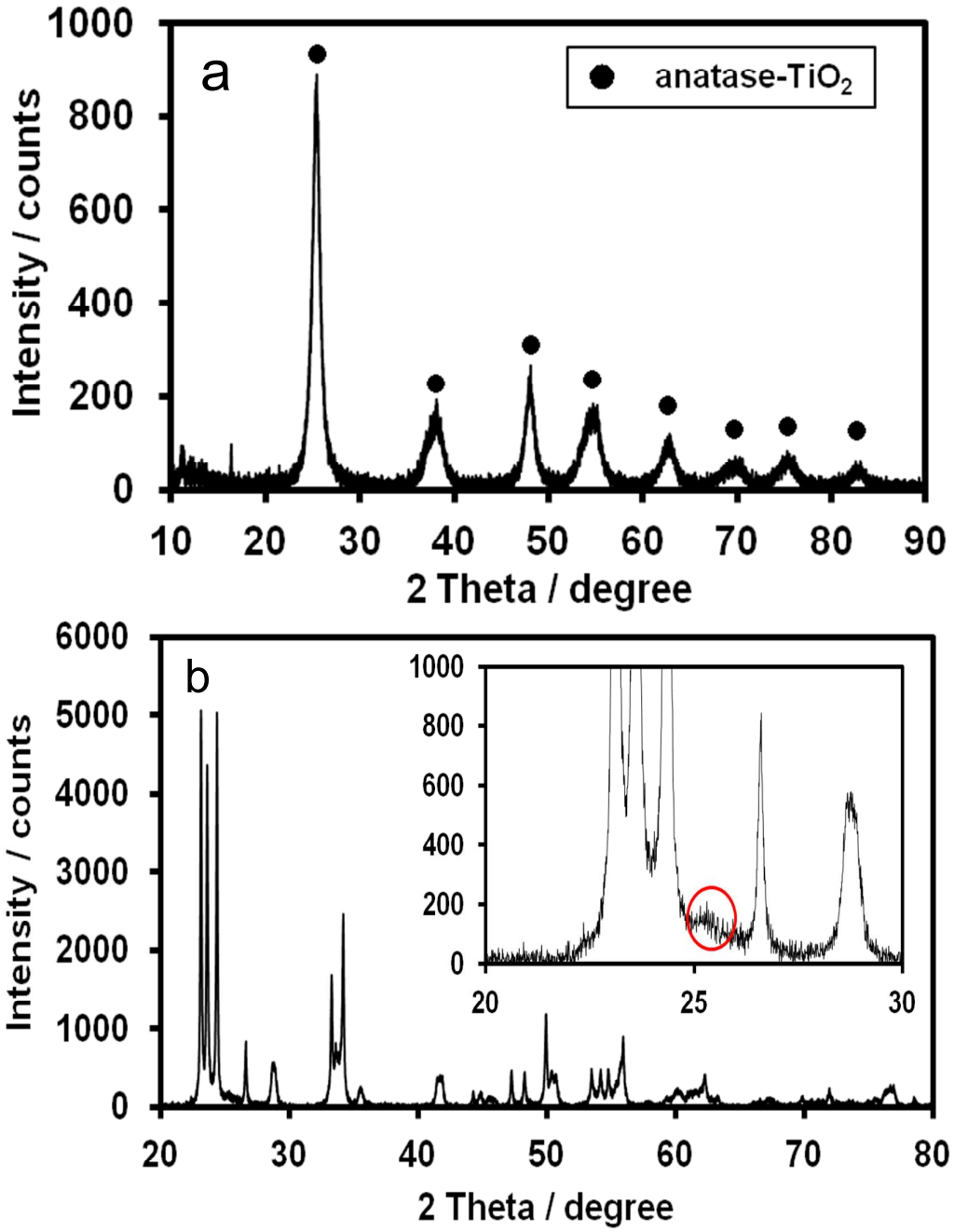

Fig. 3 X-ray powder diffraction pattern of (a) dried TiO_2 sol and (b) Pt/WO_3-TiO_2. Inset shows the magnified pattern and the red circle indicates the main diffraction peak of the anatase TiO_2 phase.

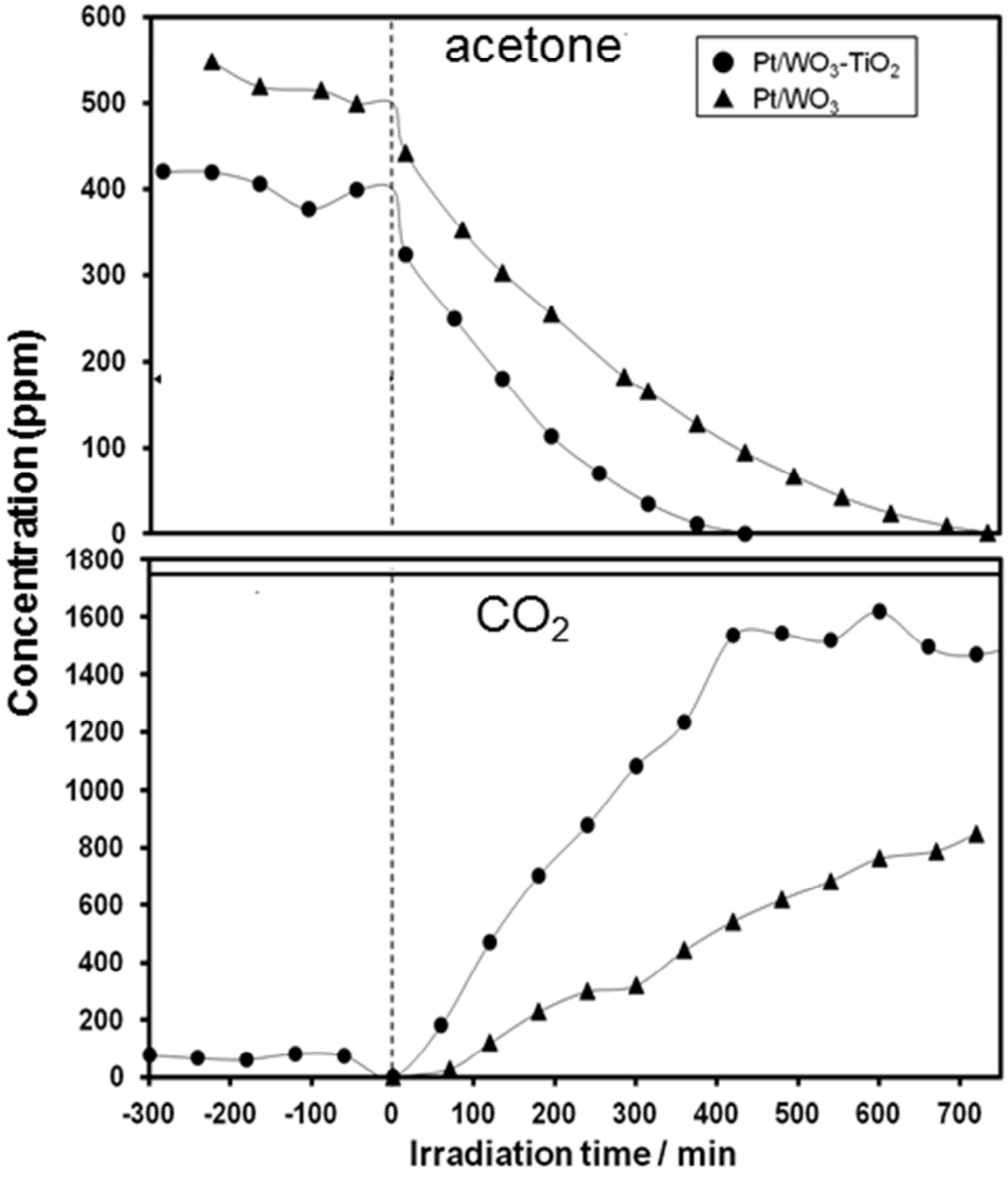

Fig. 4 Time courses of acetone and CO_2 concentrations during the photocatalytic reaction.

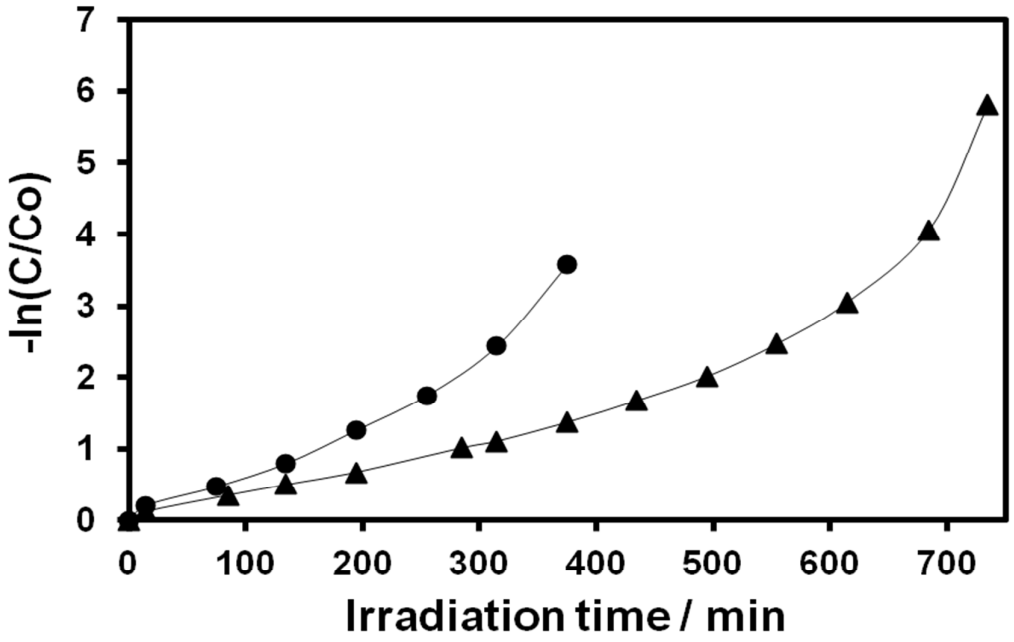

Fig. 5 First order plot of acetone concentration during the photocatalytic reaction. Solid circles; Pt/WO_3-TiO_2, solid triangles; Pt/WO_3.

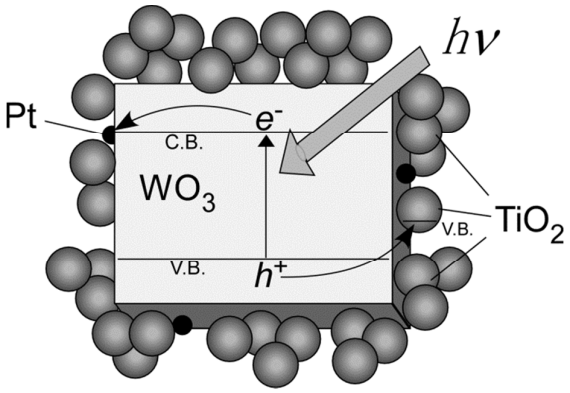

Fig. 6 Schematic illustration of composite photocatalyst.